A DETERMINISTIC NEAR-FIELD SOURCE MODEL

by

JAMES H. DIETERICH[I]

SYNOPSIS

Computations for the quasi-static and transient deformations of earthquakes on a pre-existing fault are performed with plane strain and three-dimensional finite element models. Results of the computations offer a basis for prediction of the dependence of displacements and near-field transient motions on stress drop, rupture dimensions and seismic energy. Scaling laws evaluated with the computational results are in good agreement with the observed earthquake data. The earthquake data show that ground motions and source parameters are functions of earthquake magnitude, but there is considerable scatter. The scaling indicates that more precise predictions for potentional ground motions and source parameters may be obtained using stress drop and source dimensions.

INTRODUCTION

At the National Center for Earthquake Research of the United States Geological Survey deterministic two- and three-dimensional finite element models have been developed that simulate earthquake sequences arising from slip on pre-existing faults. Computations are performed for the quasi-static displacements fields that occur between earthquake events and for the acceleration fields at repeated intervals during simulated earthquakes. Results of studies with these models are currently being applied to questions pertaining to the prediction of earthquake source parameters and ground motions for engineering design applications.

Prediction of potential ground motions must ultimately rely on evaluations of observational data from past earthquakes. However, these data are incomplete and show large amounts of scatter. As a result, direct interpretations of the data to yield characterizations of ground motions as a function of earthquake magnitude have been subject to considerable uncertainty. The computational models are used to examine the processes that control source parameters and near field transient motions. This approach provides a framework for analysis of the data in terms of parameters that characterize the earthquake source.

MODEL AND ANALYSIS

The computational model for seismic faulting consists of an elastic body with an initially planar fault. The model employs static and sliding friction as the principal variables that control fault slip. The friction parameters may vary with location on the fault surface. Boundary displacements which increase with time elastically distort the body and

[I] National Center for Earthquake Research, U.S. Geological Survey, Menlo Park, California 94025, U.S.A.
Publication authorized by the Director, U.S. Geological Survey.

induce slip. An earthquake event occurs when the stress at some point exceeds the assigned static friction. The acceleration fields during an event are determined by performing a step-by-step forward integration. As the rupture propagates, stationary points along the fault begin to slip only when the load exceeds the static strength.

The computational approach employs the finite element method and follows an analysis previously used to simulate earthquakes and aftershocks in a one-dimensional fault model (1). The finite element mesh used for the three-dimensional analysis is illustrated by Fig. 1. The shaded surface aa'cc' in Fig. 1 represents the fault. The model is composed principally of linear strain elements that have the shape of a cube. The material immediately adjacent the fault consists of composite elements built up of averaged constant strain tetrahedra. Because uniform elastic properties are assumed and the fault is taken to be initially planar, it is necessary to treat the material on only one side of the fault. The model has been given periodicity in the x-direction to avoid undersired complications that would arise if the ends of the model were either free or somehow constrained. The effect of the periodicity condition is to preserve continuity across the ends of the model abcd and a'b'c'd'. The top of the prism aa'bb' corresponds to the surface of the earth and is a free surface. The back and undersurface of the model, bb'dd' and cc'dd', respectively, are surfaces on which any system of boundary conditions may be applied to deform the body. For the results, presented below, uniform displacements in the x-direction are applied on bb'dd' with the y- and z-components of displacement held fixed at zero and on cc'dd' the z-component of displacement is also specified as zero. The fault displacements are predominately strike-slip.

The two-dimensional model is essentially the plane strain equivalent of the three-dimensional model. It treats the deformations of a slice perpendicular to the fault and parallel to the direction of slip. The computations retain the periodicity parallel to the fault and employ a regular mesh of triangular constant strain elements.

For the quasi-static deformations the displacements of the nodal points of the finite element mesh are determined from a system of simultaneous equations which have the form:

$$\{F\} = [K]\ \{\delta\} \qquad (1)$$

where $\{F\}$ is a vector array which lists the components of the total force acting at each mode, $\{\delta\}$ is the corresponding vector array of nodal displacements and $[K]$ is the stiffness matrix. Procedures for determination of $[K]$ are described in the standard references for the finite element method (2).

For the solution of a specific problem, displacement and force boundary conditions are incorporated directly into $\{\delta\}$ and $\{F\}$. For static analysis of the fault models, nodes along the fault are not permitted to slip but warping of the fault is allowed by holding the component of force perpendicular to the fault constant on the fault surface. A seismic event begins when the component of force acting parallel to the fault at a fault node equals the static strength of the node.

When a fault node slips during a seismic event the force acting on the node is opposed by the sliding friction. Therefore, force boundary conditions are operative on nodes along the fault that are moving. Applying the principle of d'Alembert, the dynamic problem is reduced to the static case by introducing the forces due to the accelerations of the nodes. Adding the dynamic force to (1) yields

$$\{F\} = [K]\ \{\delta\} + [M]\ \{\ddot{\delta}\} \qquad (2)$$

where $\{\ddot{\delta}\}$ represents the nodal accelerations and [M] is the mass matrix.

The variation with time of the accelerations is determined from (2) by performing a stepwise forward integration using the method of Wilson and Clough (3). It is assumed that the accelerations vary linearly between time steps of duration Δt. A system of simultaneous equations for the unknown accelerations $\ddot{\delta}^{t+\Delta t}$ may be derived using $\dot{\delta}^{t}$ and $\ddot{\delta}^{t}$ from the preceding time step:

$$\{C\} = [D]\ \{\ddot{\delta}^{t+\Delta t}\} \qquad (3)$$

where

$$\{C\} = \{F\} - [K]\ (\{\delta^{t}\} + \Delta t\ \{\dot{\delta}^{t}\} + \frac{\Delta t^2}{3}\ \{\ddot{\delta}^{t}\}) \qquad (4)$$

$$[D] = [M] + [K]\ (\frac{\Delta t^2}{6})$$

Solution of the simultaneous equations (3) yields the unknown acceleration field at the end of time step Δt. After each time step the velocities and displacements are computed from the accelerations. The force acting on each stationary fault node is determined and if the force exceeds the static friction the node is allowed to begin movement during the next time step. Similarly if the velocity of a moving fault node has gone to zero during the preceding time step, the node is then held stationary until the force again exceeds the static friction. Thus repeated solutions for the acceleration field are obtained until all fault nodes cease to move. A static solution is then obtained to determine the static equilibrium displacements at the end of the event.

It is seen that if the boundary displacements are allowed to increase continuously with time then sequences of rupture events may be simulated. If the friction along the fault is irregular the displacements during a rupture event will not be uniform and generally slip will occur on only a portion of the fault. Because of the resulting stress concentrations, successive events occur at different locations and tend to vary in size. At present it is practical to simulate sequences of earthquakes only with the plane strain model.

SCALING

The terms in equations (1) through (4) are derived from parameters that specify the grid dimensions, stresses, elastic constants and density. The computations may be performed with arbitrarily assigned values for these parameters and then scaled for any specifically desired set of values. The scaling is significant because it allows results for source parameters and transient motions to be scaled in terms of the other source parameters,

stress, elastic constants and density.

If ℓ' is a length parameter which characterizes the size of the finite element grid and ℓ similarly characterizes the dimensions of the grid for which a solution is desired then the scaling factor a is defined by:

$$a = \ell/\ell' \tag{5}$$

Similarly b, c and d are defined as the scale factors for stress, σ, elastic constants, μ, λ and density, ρ, respectively.

$$b = \sigma/\sigma' \tag{6}$$

$$c = \mu/\mu';\ \lambda/\lambda' \tag{7}$$

$$d = \rho/\rho' \tag{8}$$

It is noted that the friction parameters determine the magnitudes of stress and therefore also scale with (7). The Lamé elastic parameters μ and λ scale together and therefore assume a constant Poisson's ratio. A Poisson's ratio of .25 was employed for the computations presented here.

By inspection, the following relationships are obtained for the terms in equations (1) through (4).

$$\{F\} = \{F'\}\ a^2 b \tag{9}$$

$$[K] = [K']\ ac \tag{10}$$

$$\{\delta\} = \{\delta'\}\ abc^{-1} \tag{11}$$

$$[M] = [M']\ a^3 d \tag{12}$$

$$[D] = [D']\ a^3 d \tag{13}$$

$$\{C\} = \{C'\}\ a^2 b \tag{14}$$

$$\{\dot{\delta}\} = \{\dot{\delta}'\}\ bc^{-1/2}\ d^{-1/2} \tag{15}$$

$$\{\ddot{\delta}\} = \{\ddot{\delta}'\}\ a^{-1} bd^{-1} \tag{16}$$

$$\Delta t = \Delta t'\ ac^{-1/2}\ d^{1/2} \tag{17}$$

Following the convention introduced above the unprimed quantities refer to the scaled values. From equations (9) through (17) scaling laws may be derived that expresses the relationships between the source parameters and conditions at the earthquake source. These scaling laws may also be obtained independent of the computational model by the method of dimensional analysis.

RESULTS

Source parameters that describe the characteristics of the simulated earthquakes include rupture dimensions, displacements, stress drop, seismic energy and seismic moment. Stress drop, $\Delta\tau$, is defined here as the difference between the average initial shear stress, τ, on the rupture surface and the average final shear stress τ_1. For scaling, the magnitude of $\Delta\tau$ varies with the magnitude of τ as given by equation (6), while the

fractional stress drop $\Delta\tau/\tau$ which is dimensionless remains constant for a fixed ratio of static friction to sliding friction. The displacement, D, represents the average relative displacement across the fault. Because rupture length, L, scales by (5) and stress drop scales by (6) L and $\Delta\tau$ may be substituted for the parameters ℓ and σ in (5) and (6). When this is done it follows from (11) that

$$D = K_1 \Delta\tau L/\mu \tag{18}$$

where K_1 is a numerical constant which is evaluated from:

$$K_1 = D'\mu'/\Delta\tau' L' \tag{19}$$

Values obtained for K_1 and the other numerical constants employed in the following equations are given in Table I.

The total change of strain energy, E_T, associated with an event is obtained from the static displacement fields immediately before and after the event. In computing E_T the strain energy obtained from the model is multiplyed by two so as to account for the two sides of the fault and in the two-dimensional models the depth of the rupture is assumed to be two-thirds the length. Work done in sliding, W, is obtained from slip on the fault and the sliding friction; again taking into account each side of the fault and, in the two-dimensional models, the assumed depth of rupture. Seismic energy, E_S, is then obtained from:

$$E_S = E_T - W \tag{20}$$

Energy terms scale by the product of force by displacement hence:

$$E_S = E_S' \, a^3 b^2 c^{-1} \tag{21}$$

Once again L and $\Delta\tau$ are used to characterize ℓ and σ in (5) and (6) to obtain:

$$E_S = K_2 \, L^3 \Delta\tau^2/\mu \tag{22}$$

Combining (21) with (18):

$$E_S = K_3 L D^2 \mu \tag{23}$$

Seismic moment, M_o, is defined by Aki (4) as:

$$M_o = \mu A D \tag{24}$$

where A is the area of the rupture. Because A scales by L^2:

$$M_o = K_4 \mu L^2 D \tag{25}$$

where K_4 is a simple geometric parameter relating L to A. Combining (23) with (25) we obtain:

$$E_S = K_5 M_o^{\,2}/\mu L^3 \tag{26}$$

The scaling laws (22), (23) and (26) are presented graphically in Fig. 2 which plots E_S against L for different values of $\Delta\tau$, D and M_o. The values for K_2, K_3 and K_5 used for locating the curves in Fig. 2 are from the two-dimensional multi-event simulations. Seismic energy in Fig. 2 has been equated to surface wave magnitude M_S following the energy-magnitude relation of Gutenberg and Richter (5). Approximate local

magnitude M_L is also indicated in Fig. 2.

Figure 2 illustrates the hazards of attempting to characterize source parameters such as L or D simply in terms of earthquake magnitude. Any such characterization will carry the assumption that either stress drop is the same for all earthquakes or that stress drop varies regularly with magnitude. Stress drop data for earthquakes show considerable scatter and provide scant indication of regular variation with magnitude Chinnery (6). For purposes of comparison, observed earthquake data primarily from the list compiled by King and Knopoff (7) are plotted in Fig. 2 along with the magnitude-length correlations suggested by Press (8) and Wyss and Brune (9). When plotted for length and magnitude the observed fault displacements agree very well with the values predicted by the model. Stress drop data shows somewhat greater scatter than the displacement data because of the dependence of stress drop on the fault width. This is especially important for the larger earthquakes which tend to have small widths when compared to length. Use of the three-dimensional results in Fig. 3 would presumably improve the agreement with the stress drop data.

From (15) any particle velocity, $\dot{\delta}$, for the simulated earthquakes scales by:

$$\dot{\delta} = K\Delta\tau\beta/\mu \qquad (27)$$

where β is the shear velocity. In (27) $\Delta\tau$ may represent either the stress drop or, perhaps more appropriately, the driving stress of the rupture which is the difference between the shear stress at the instant rupturing commences and the sliding friction. If driving stress is employed, equation (27) is equivalent to the relationship derived by Brune (10) for initial particle velocity on the fault.

Figure 3 gives the peak horizontal velocity for bilateral rupture events in the three-dimensional models along profiles that extend perpendicular to the fault from the point of initial slip. Because length does not enter (27), the distances in Fig. 3 are arbitrary and may be expressed in terms of rupture dimensions. The amplitude curves for finite ruptures are flat near the fault and decrease by approximately $(\text{distance})^{-1}$ at greater distances. The dependence of the "corner" distance of the velocity profiles on the minimum rupture dimension, L_m, is demonstrated by model 7 which is for a propagating rupture whose dimensions were allowed to increase during the entire simulation. The curve for model 7 is essentially flat. Because rupture dimensions scale with distance, the corner distance for the velocity profiles is characteristic of L_m which in the three-dimensional models presented here, is the fault depth, W.

Figure 4 gives the peak velocity versus distance data compiled by Page and others (11) for magnitude 5.0 to 7.7 earthquakes. These data show great scatter as might be expected from the dependence of the velocity profiles on stress and rupture dimensions.

In Fig. 5 these data have been parameterized using observed or inferred stress drop and minimum rupture dimension. Where direct observations for the source parameters of the earthquakes are not available, a 10-bar stress drop was assumed and a minimum rupture

dimension was inferred from the magnitude-length plot in Fig. 2. Reducing the data in this manner substantially decreases the scatter and allows for comparisons with the numerical results.

Figure 6 gives the peak horizontal accelerations in the three-dimensional models along the profiles used for discussion of the velocity data. The variation of acceleration with distance is similar to that observed for velocity. Near the fault the accelerations are uniform while at a distance characteristic of L_m the accelerations begin to decrease by approximately $(\text{distance})^{-1}$. The slight decrease with distance of the accelerations for model 7 is believed to be fictitious because it may be accounted for entirely by the lengthening of the higher frequency waves as they propagate through the relatively coarse mesh.

From (16) accelerations scale by

$$\ddot{\delta} = K\Delta\tau/\ell\rho \qquad (28)$$

Because of the dependence of (28) on ℓ which is a measure of the highest frequency that the mesh may transmit, the peak acceleration is proportional to frequency ω, raised to the first power. Specifically, from (28) and (17)

$$\ddot{\delta} = K\Delta\tau\omega\beta/\mu \qquad (29)$$

Figure 7 plots the peak acceleration data from Page and others (11). Following the procedure followed for the velocity data, the accelerations have been parameterized using stress drop and L_m and compared with the model results in Fig. (8). Because the recorded data have a high frequency cutoff of approximately 10 Hz the model data have been scaled following (29) for 10 Hz. The parameterization of the data significantly reduces the scatter and shows that the model results are in good agreement with the observations. The apparent decrease of accelerations at a rate greater than $(\text{distance})^{-1}$ shown by the data presumably arises from attenuation which is not treated in the computation.

REFERENCES

(1) Dieterich, J. H., Time-dependent friction as a possible mechanism for aftershocks, J. Geophys. Res., 77, 3771-3781, 1972.

(2) Zienkiewicz, O. C., The Finite Element Method in Engineering Science, McGraw-Hill, London, 1971.

(3) Wilson, E. L., and R. W. Clough, Dynamic response by step-by-step matrix analysis, in Symposium on the Use of Computers in Civil Engineering, Lisbon, October, 1962, paper 45, pp. 1-14, Laboratorio National de Engenharia Civil, Lisbon, Portugal, 1962.

(4) Aki, K., Generation and propagation of G waves from the Niigata earthquake of June 16, 1964, Part 2. Estimation of earthquake moment, released energy and stress-strain drop from G-wave spectrum, Bull. Earthquake Res. Inst., Tokyo Univ., 44, 73-88, 1966.

(5) Gutenberg, B., and C. F. Richter, Magnitude and energy of earthquakes, Ann. Geofisics, 9, 1-15, 1956.

(6) Chinnery, M. A., Theoretical fault models, in Symposium on Processes in the Focal Region, Publications of the Dominion Observatory,

37, no. 7, 211-223, 1969.
(7) King, C.-Y. and L. Knopoff, Stress drop in earthquakes, Bull. Seism. Soc. Am., 58, 249-257, 1968.
(8) Press, F., Dimensions of the source region for small shallow earthquakes, in Proceedings of VESIAC Conference on Shallow Source Mechanisms, VESIAC Report 7885-1-X, 155-163, 1967.
(9) Wyss, M. and J. N. Brune, Seismic moment, stress and source dimensions for earthquakes in the California-Nevada region, J. Geophys. Res., 73, 4681-4694, 1968.
(10) Brune, J. N., Tectonic stress and the spectra of seismic shear waves from earthquakes, J. Geophys. Res., 75, 4997-5009, 1970.
(11) Page, R. A., D. M. Boore, W. B. Joyner and H. W. Coulter, Ground motion values for use in the seismic design of the Trans-Alaska pipeline system, U.S. Geological Survey Circular 672, 23 p., 1972.

TABLE I

Model	K_1	K_2	K_3	K_4	K_5
(1) 2D uniform bilateral rupture	1.06	.393	.355	.667	.799
(2) 2D average of 26 events from multi-event simulations with variable friction	1.19	.204	.223	.667	.501
(3) 3D uniform rupture propagating from free surface length = 4.0, width = 1.0	1.61	.243	.933	.250	1.49
(4) 3D uniform rupture propagating from free surface length = 4.0, width = 1.5	.860	.119	1.61	.375	1.17
(5) 3D uniform rupture propagating from depth = 0.5, length = 4.0, width = 1.5	.846	.123	1.74	.375	1.23
(6) 3D uniform rupture propagating from depth = 0.5, length = 4.0, width = 2.0	1.62	.414	1.59	.500	.636

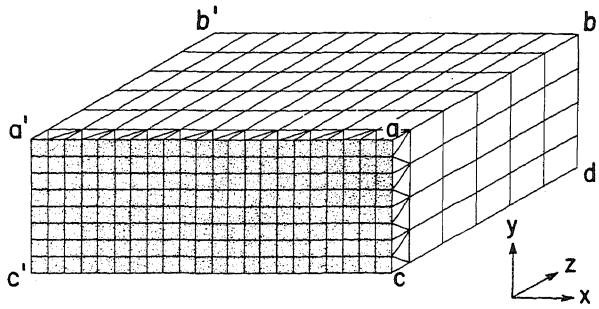

Figure 1. Three-dimensional finite element model used for earthquake simulation. The shaded area aa'cc' represents the fault.

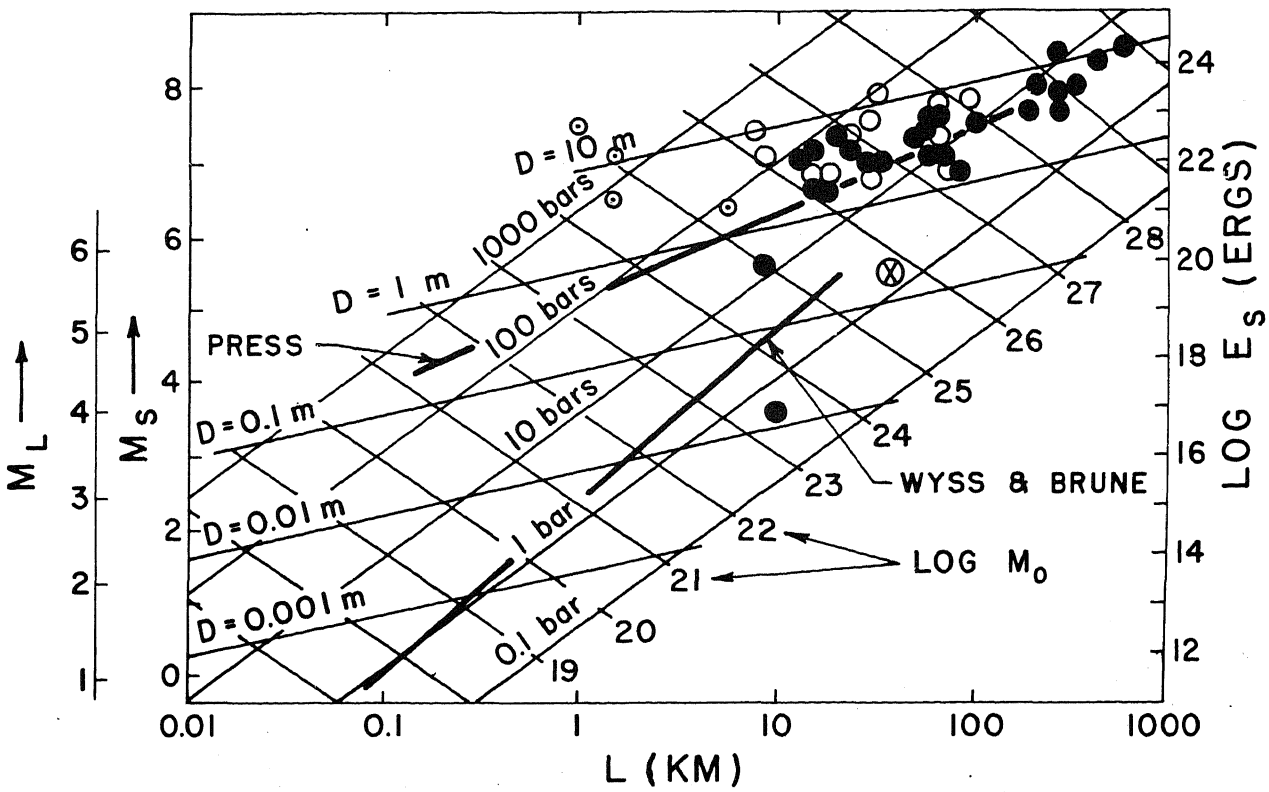

Figure 2. Summary of computed strain energy E_S, rupture length, L, average fault offset, D, stress drop, $\Delta\tau$, and seismic moment, M_o, evaluated for the plane strain model with μ, $\lambda = 2.5 \times 10^{11}$ dynes/cm^2 and $\rho = 3.0$ gm/cc. M_L and M_S are the inferred local and surface wave magnitudes that correspond to E_S. Earthquake data from King and Knopoff (7) are plotted by magnitude and rupture length. Agreement of the observed and computed fault displacements by less than a factor of two, between a factor of two and five and greater than a factor of five is indicated by the solid circles, large open circles and the open circles with dots, respectively. The circle with an X represents the 1966 Parkfield earthquake which has estimates of displacement of .05 m and .5 m.

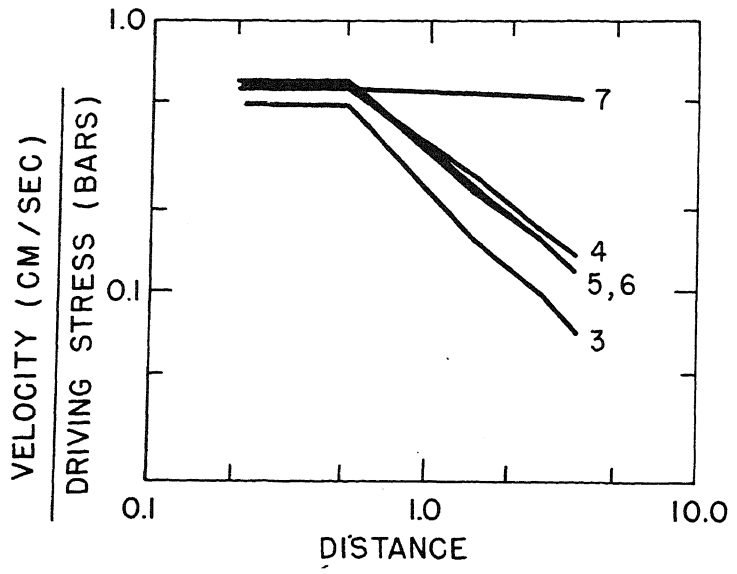

Figure 3. Peak horizontal velocity versus distance for the three-dimensional models with μ, λ = 2.5 x 10^{11} dynes/cm^2 and ρ = 3.0 gm/cc. The rupture length of models 3 through 6 is 4 (units arbitrary) with the rupture widths, given in Table I. The rupture in model 7 continued to propagate during the entire simulation.

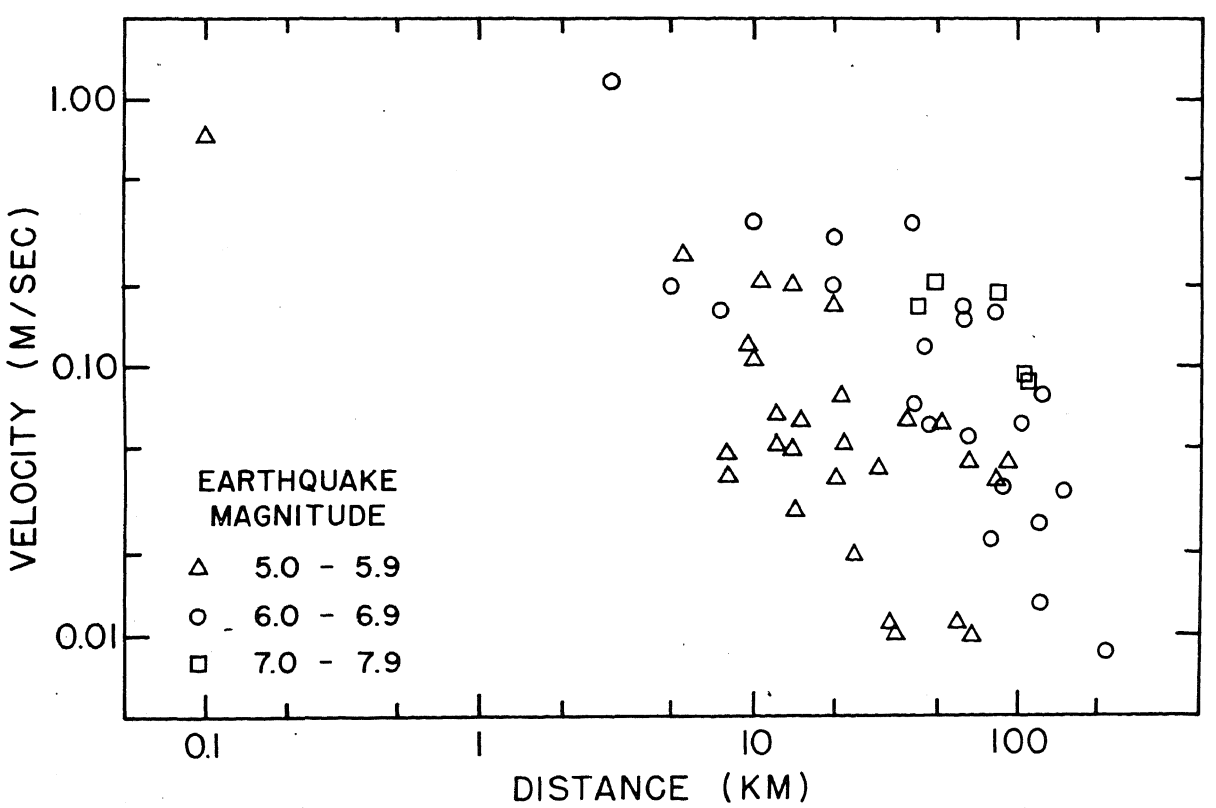

Figure 4. Peak velocity versus distance for earthquakes of magnitude 5, 6 and 7. Data is from Page and others (11).

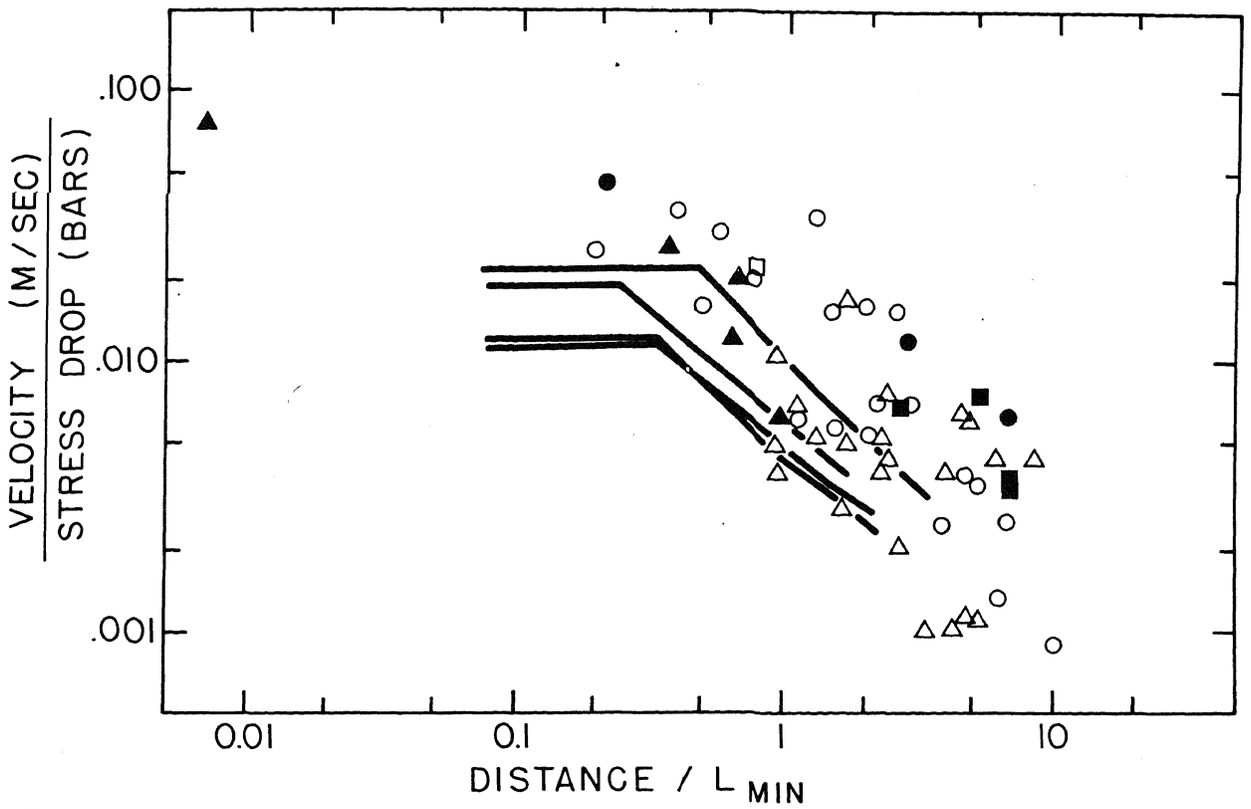

Figure 5. Parameterization of peak velocity and distance using stress drop and minimum rupture, dimension, L_{min}. The data from Figure 4 are replotted using an assumed magnitude-length relationship (open symbols) or the known rupture dimensions (solid symbols).

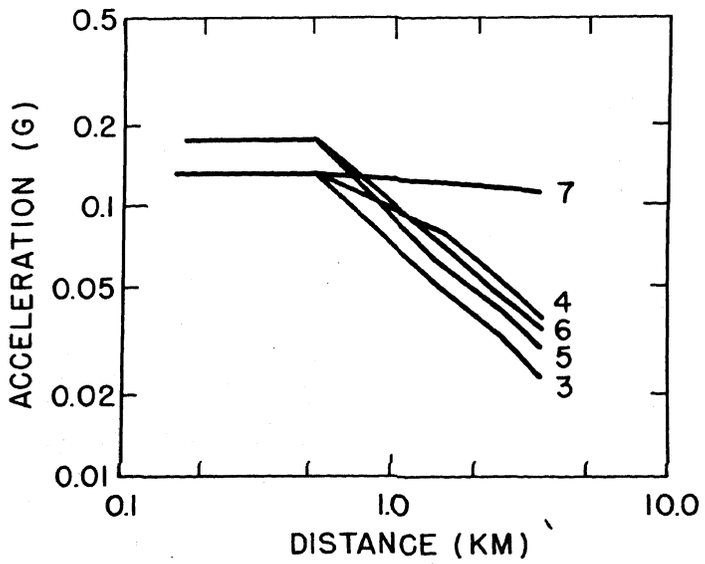

Figure 6. Peak horizontal acceleration versus distance for the three-dimensional models with μ, $\lambda = 2.5 \times 10^{11}$ dynes/cm^2 and $\rho = 3.0$ gm/cc. The rupture length for models 3 through 6 is 4 km. The rupture in model 7 continued to propagate during the entire simulation. The highest frequency is approximately 1.0 Hz. The driving stress is 100 bars.

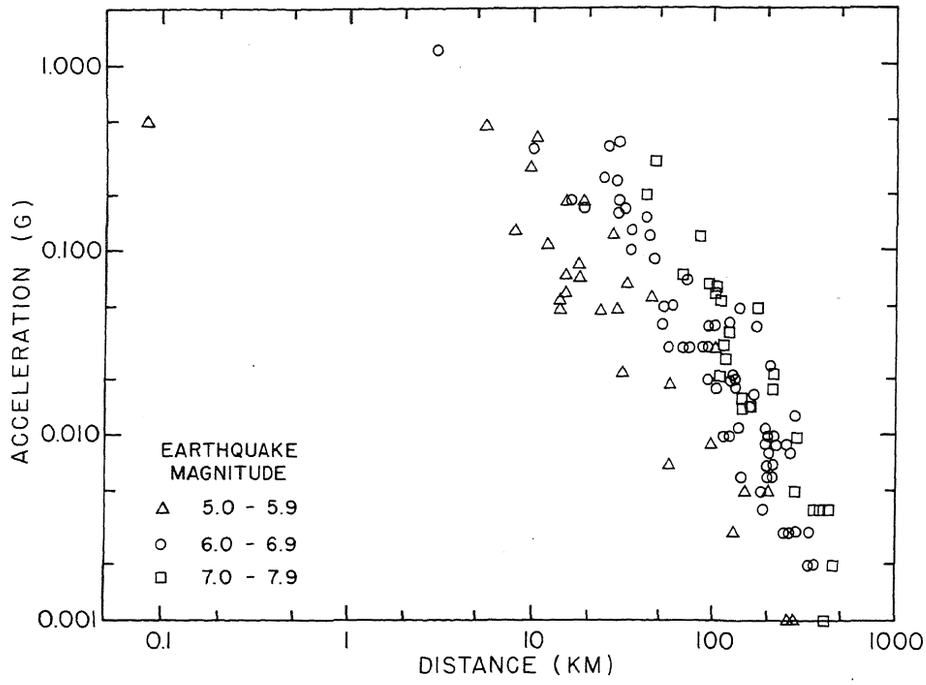

Figure 7. Peak horizontal acceleration versus distance for earthquakes of magnitude 5, 6 and 7. Data is from Page and others (11).

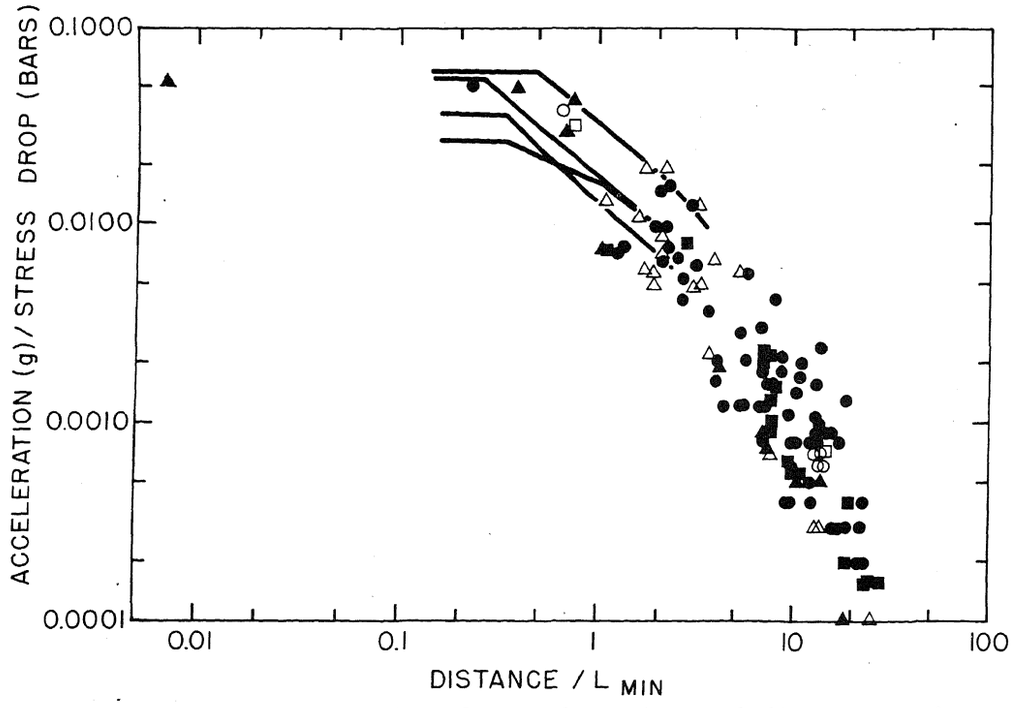

Figure 8. Parameterization of peak acceleration and distance using stress drop and L_{min}. The data from Figure 7 are replotted employing an assumed magnitude-length relationship (open symbols) or the known rupture dimensions (solid symbols). The model results have been scaled for the high frequency cutoff of approximately 10 Hz implicit in the earthquake data.